Laser Beam Welded Nickel Aluminum Bronze (Cu-9Al-4Fe-4Ni)

Laser beam welding is effective in producing narrow heat-affected zones in nickel-aluminum-bronze material

BY K. PETROLONIS

ABSTRACT. Three-eighths-inch (0.953-cm) thick plates of wrought nickel aluminum bronze (Cu-9Al-4Fe-4Ni) were autogenously laser beam welded in a butt-joint configuration using varying process parameters. The parameters that were varied include incident laser power and welding speed.

Macrophotography, light microscopy, scanning electron microscopy (SEM), and microhardness profiles have been employed to characterize the microstructures that develop in the laser beam weldments and heat-affected zones of a nickel aluminum bronze (NAB). The investigation has also documented the microstructural characteristics of the base plate prior to welding.

The weld metal is primarily martensitic but does contain proeutectoid Widmanstätten α (the copper-rich FCC solid solution). In general, the structure of the weld zone is equiaxed, although columnar grains are observed in the vicinity of the fusion line. Mixed proeutectoid α and martensite develop in the heat affected zone (HAZ) and are strongly influenced by the microstructure of the base plate. Finally, the base plate of the wrought NAB plates is composed of alternating bands of proeutectoid α which contains κ_{iv} particles, and the eutectoid mixture of $\alpha + \kappa_{iii}$. The secondary phases, referred to as κ_{iii} and κ_{iv} are based on NiAl and Fe_3Al, respectively.

Finally, some preliminary results on continuous cooling studies from the single phase β region have shown that proeutectoid α is the active nucleus for the eutectoidal reaction.

K. PETROLONIS is with the Department of Materials Science and Engineering, The Pennsylvania State University, University Park, Pa.

Paper presented at the 73 AWS Annual Meeting, held March 22-27, 1993, in Chicago, Ill.

KEY WORDS

Laser Beam Welding
Ni-Al Bronze
Cu-9Al-4Fe-4Ni
Incident Laser Power
Welding Speed
Microstructure
Wrought NAB Plates
NAB
Microhardness

Introduction

Nickel aluminum bronzes (NABs) have been in use for many years in marine applications. This material, according to Culpan and Foley (1982), is important because it exhibits a strength and corrosion resistance similar to that of medium carbon steel. Other valuable properties include: 1) low magnetic permeability, 2) low coefficient of friction, 3) resistance to softening at elevated temperatures, and 4) nonsparking nature (Culpan and Foley, 1982).

One problem that does occur, particularly in the HAZ of the arc weldments of NAB, is selective phase corrosion (Lorimer, *et al.*, 1986). Selective phase corrosion is a specific form of dealloying, the process whereby one constituent of an alloy is preferentially removed, leaving behind an altered residual structure (Fontana, 1986). Since this selective phase corrosion tends to occur in or near the HAZ, laser beam welding of the NAB material is being studied to optimize welding parameters and reduce the width of the HAZ. Laser beam welding was chosen for such a project because of the low heat inputs and rapid cooling rates associated with it. These characteristics alone would help to reduce the width of the HAZ. The ultimate aim of this project is to optimize the laser welding parameters of NAB to achieve a narrow HAZ, full penetration of the plate, and to maintain the mechanical properties of the material through microstructural control. Details of the selective phase corrosion of the laser welded NAB are presented elsewhere (Bell, 1993).

Experimental

Hot-rolled, NAB plates with the measured composition as shown in Table 1 were autogenously laser beam welded with a 14-kW continuous wave carbon dioxide laser. Details of the phase transformations that occur in hot-rolled NAB samples are provided elsewhere (Petrolonis, 1993 and Bell, 1993).

Fourteen bars (30.48 X 5.08 X 0.953 cm/12 X 2 X ⅜ in.) of the above composition were obtained. Pairs of bars were placed side-by-side and a sacrificial-cast, NAB backing strip (reinforcing strip) was tacked along the "butting" line. The backing strip was needed because the NAB tends to "drop through" during the weld-

Table 1—Alloy Composition (wt%)

Al	Fe	Ni	Mn	Si	Pb	Cu
9.20	3.76	4.50	1.35	0.04	0.01	balance

Table 2—Summary of the weld parameters

Pass #	Laser Power (kW)	Welding Speed (cm/min)	Heat Input (kJ/cm)
1	10.6	50.8	12.52
2	11.7	50.8	13.82
3	11.7	50.8	13.82
4	10.8	50.8	12.76
5	14.1	101.6	8.33
6	14.1	101.6	8.33
7	13.1	76.2	10.31
8	13.1	76.2	10.31
9	13.1	101.6	7.74
10	13.1	127	6.19
11	13.3	127	6.28
12	13.6	152.4	5.35
13	13.3	152.4	5.24
14	13.3	177.8	4.49

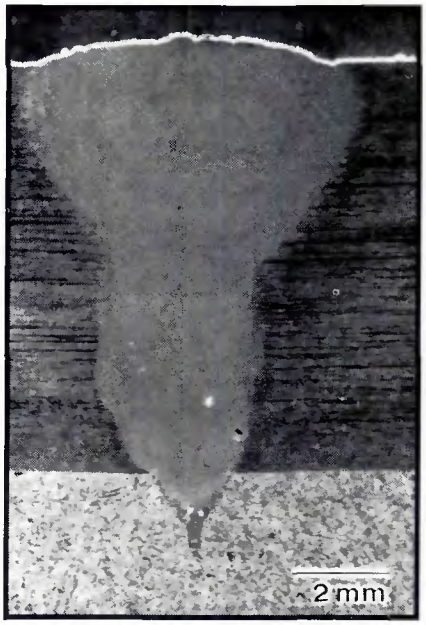

Fig. 1 — Macrograph of a laser beam weldment, 12.52 kJ/cm. Etchant: Ammonium persulfate. (Wrought NAB plate.)

ing process due to its low viscosity. The bars were then welded together using a 14-kW CO_2 laser. Two near 15-cm (6-in.) welds were made on each of the fixtured bars; thus, a total of fourteen different welds were made for subsequent analyses. The incident laser power was varied between 10.6 and 14.1 kW (see Table 2). The welding speed ranged from 50 to 178 cm/min (20 to 70 in./min). At this point, it should be noted that full penetration of the plate was achieved in over half of the welds, and a representative example is given in Fig. 1.

Light Microscopy

Standard metallographic analysis was performed. The welds were sectioned normal to the weld direction using an automated, water-cooled, abrasive cut-off wheel. The samples were then mounted in Struer's Epoxy and ground using progressively finer grit silicon carbide papers (80, 240, 320, 400, and 600) using standard metallographic practices. Polishing of the samples was then performed using 600-grit alumina powder. The samples were etched in either 10 g ammonium persulfate in 90 mL of distilled water or a mixture containing equal volumes of ammonium hydroxide, hydrogen peroxide and distilled water.

Scanning Electron Microscopy (SEM)

The samples were removed from the mount so that the mount would not charge under the action of the electron beam.

The samples that were etched in am-

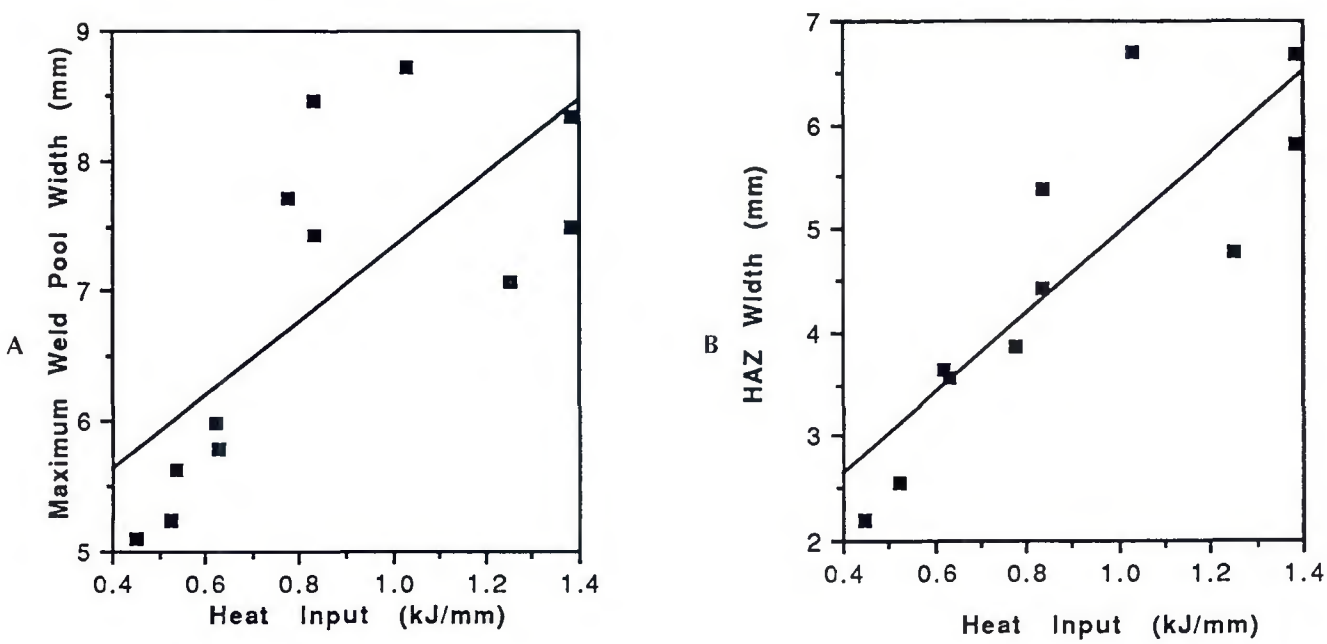

Fig. 2 — A — Plot of fusion zone width vs. heat input; B — plot of the HAZ width at 50% penetration vs. heat input.

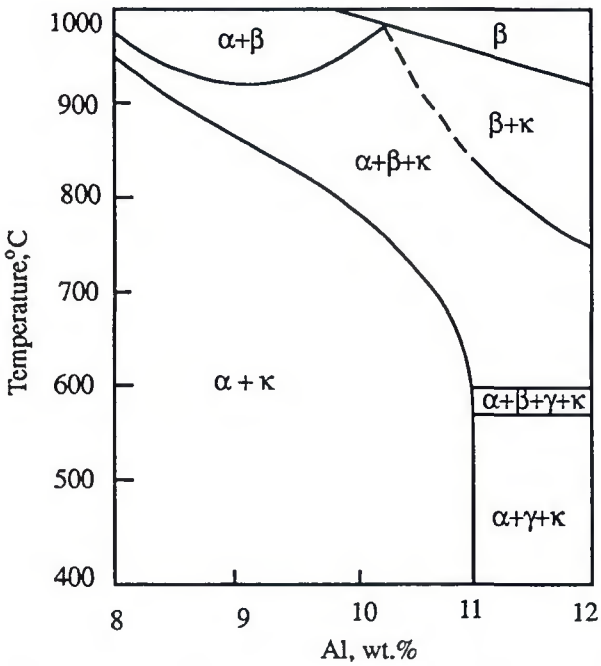

Fig. 3 — Vertical section of the Cu-Al-5%Ni-5%Fe phase diagram (Cook, et al., 1951-52).

Fig. 4 — Low-magnification SEM micrograph of the fusion line (heat input = 12.52 kJ/cm). Etchant: Ammonium hydroxide solution.

Fig. 5 — SEM micrograph showing microstructural banding and representative phases of the wrought base plate. Etchant: Ammonium hydroxide solution.

monium persulfate yielded little contrast in the SEM, so the samples were repolished using 600-grit alumina powder and etched in the ammonium hydroxide, hydrogen peroxide, distilled water solution. To further enhance the contrast in the SEM, the samples were purposely overetched in this solution. In addition to this, a line of silver paint, from the metal to the sample holder, was used to prevent the sample from charging.

Microhardness

Sample preparation for microhardness included repolishing the surfaces with 600-grit alumina powder and reetching in the ammonium hydroxide, hydrogen peroxide, distilled water solution. This was performed to eliminate variations in the hardness data due to the presence of any oxide layer which might have formed during storage in air, after laser beam welding. Hardness measurements were taken every 0.5 mm, using a load of 100 grams and the Vicker's hardness indentor.

Results and Discussion

Macroanalysis of the Weldments

A typical macrograph of a laser weldment in the wrought material is shown in Fig. 1. Figure 1 also shows that a banded microstructure is maintained from the base plate up to the fusion line, although the phases present in the base plate and HAZ are dissimilar. A plot of maximum weld pool width as a function of heat input is shown in Fig. 2A, and a plot of the HAZ width at 50% penetration is presented in Fig. 2B. As might be expected, the width of both the weld pool and HAZ increase with increasing heat input. The linear fit was employed since it is well known that for the low power associated with laser beam welding, a linear relationship is expected (Lancaster, 1980). Also note that the width of the heat-affected zones generated in the laser weldments are quite narrow compared with those associated with gas metal arc welding, which are approximately 4 to 5 times the size of the HAZs associated with laser beam welding.

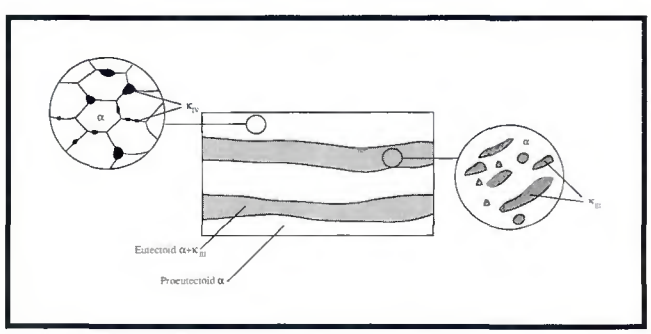

Fig. 6 — Schematic illustrating microstructural banding and the phases which are present in the wrought base plate.

Fig. 7 — SEM micrograph of the HAZ near to the fusion line illustrating the presence of martensite, as well as bands of proeutectoid α (heat input, 12.52 kJ/cm). Etchant: Ammonium hydroxide solution.

Microstructural Analysis of the Weldments

To aid in the discussion, a vertical section of the Cu-Al-5%Ni-5%Fe phase diagram is presented in Fig. 3. According to this diagram, the phases expected to be present at equilibrium are proeutectoid α and the eutectoidal mixture of α + κ (Cook, *et al.*, 1951-52). However, due to the fact that this is a quaternary system, other phases will be present, and the eutectoidal κ phase will be designated as κ_{iii} (the designation is used to provide consistency with earlier work of, e. *g.*, Hasan, *et al.*, (1987)).

Base Metal and Heat-Affected Zone

Figure 4 is a low magnification SEM image of the weld metal, HAZ, and the base plate regions. The banding, as stated above with respect to Fig. 2, is particularly evident and exists up to the fusion line. Figure 5 illustrates the microstructure present in the base plate well removed from the weld metal. Here, the microstructure is banded and consists of alternating regions of proeutectoid α and the eutectoidal mixture of α + κ_{iii} (e. *g.*, see the schematic diagram of Fig. 6). There is also a precipitate evident on the α grain boundaries and within the α-matrix which is the κ_{iv} phase (Bell, *et al.*, 1991). At this point, it can be noted that the image presented in Fig. 5 bears a remarkable resemblance to manganese-bearing hypoeutectoid steels which yield a banded ferrite/pearlite microstructure after hot-rolling and slow cooling from the austenite region (Thompson and Howell,1992).

Progressing from the base metal to the HAZ, a phase transformation occurs. In the HAZ nearest to the weld zone, all of the bands of the eutectoidal mixture α+ κ_{iii}, together with a large fraction of the proeutectoid α bands have transformed to β upon heating and subsequently to martensite upon cooling. Hence, the microstructure consists primarily of martensite bands together with predominantly proeutectoid α bands (see Fig. 7). In the HAZ further from the weld, martensite is still formed, though to a lesser degree due to the decreasing peak temperature and temperature gradient from the weld center (see Figure 8). Notice also that the proeutectoid α bands are thicker, progressing farther into the base plate away from the weld center, which implies that the martensite formed farther from the fusion line corresponds primarily to the α + κ_{iii} bands which were present prior to welding. In addition to the HAZ constituents, martensite appears within the proeutectoid α as thin plates or rods (Hasan, *et al.*, 1987).

Weld Metal

In the weld metal the microstructure adjacent to the fusion line was observed to exhibit a change in morphology from an equiaxed grain structure at the weld center (Fig. 9) to a columnar structure adjacent to the fusion line (see Fig. 10). Examination of a longitudinal section of the weld confirmed the existence of an equiaxed grain structure toward the center of the weld. It is observed that the weld metal microstructure exists primarily as Widmanstätten proeutectoid α and martensite (see Figs. 9 and 10). The Widmanstätten α forms an interlocked structure with the martensite between the rods of α. Structural identification of the martensite has been performed by, e. *g.*, Hasan, *et al.*, 1982, 1987. Another observation was that the welds produced at lower heat inputs exhibited a finer dispersion of Widmanstätten α (see Fig. 11A–C).

Microhardness

The microhardness values obtained for three welds are presented in Fig. 12 A–C. Each of these welds was run at a different heat input, as illustrated in Table 2. The highest hardness at the weld center (approximately 300 Vicker's hardness number (VHN)) is directly related to the presence of the maximum volume fraction of martensite at this location. As distance from zero (0) mm increases to both the left and right, the material generally appears to be less hard (approximately 150-250 VHN). Note, arrows in Fig. 12A–C indicate the approximate location of the fusion line. Notice also that each of the hardness plots exhibit tall stray peaks. These peaks

A

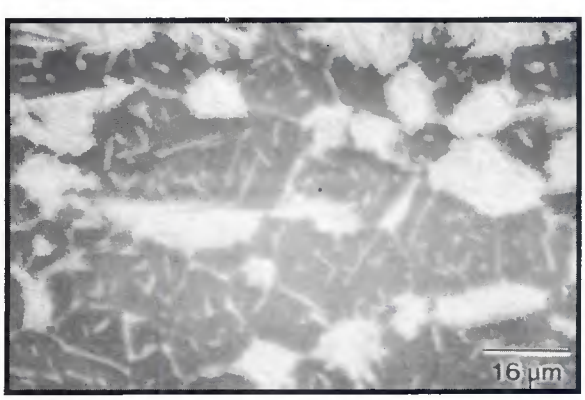

B

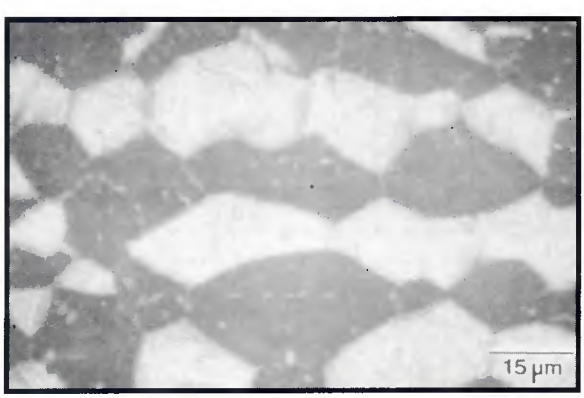

Fig. 8 — A — SEM micrograph of the HAZ away from the fusion line showing the presence of martensite and bands and proeutectoid α (heat input, 12.52 kJ/cm). Etchant: Ammonium hydroxide solution; B — SEM micrograph of the HAZ away from the fusion line showing the wider bands of proeutectoid α and less martensite (heat input, 12.52 kJ/cm). Etchant: Ammonium hydroxide solution.

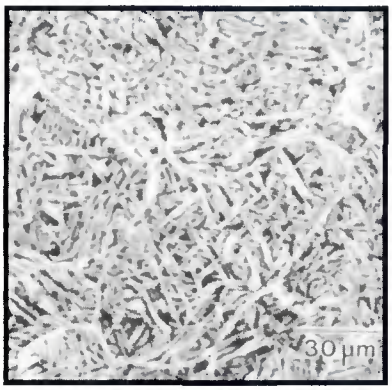

Fig. 9 — Light micrograph of the weld metal at the center of the weld zone (heat input, 12.52 kJ/cm). Etchant: Ammonium hydroxide solution.

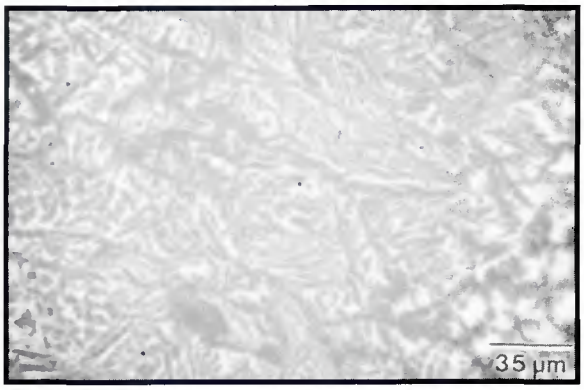

Fig. 10 — SEM micrograph, showing columnar growth near the fusion line (heat input, 12.52 kJ/cm). Etchant: Ammonium hydroxide solution.

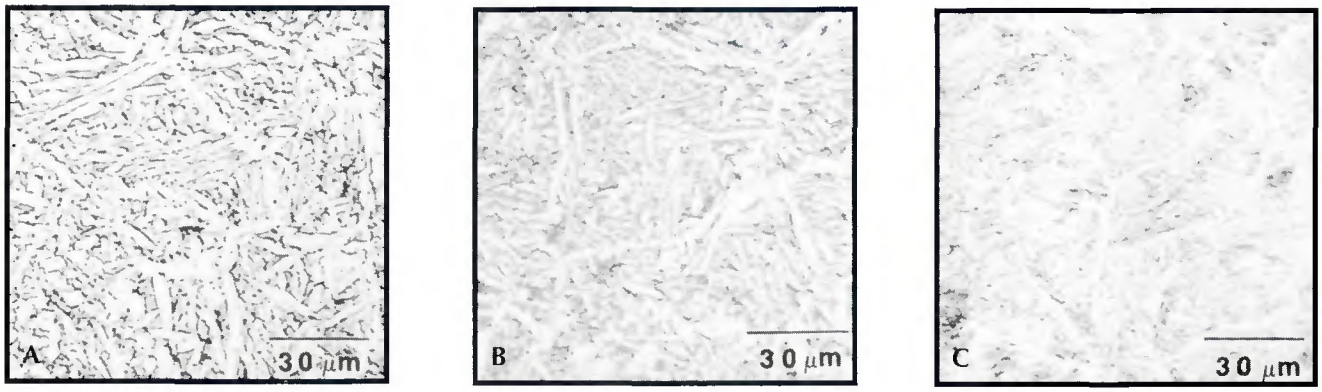

Fig. 11 — A — Light micrograph of the weld produced at a heat input of 12.52 kJ/cm; B — light micrograph of the weld produced at a heat input of 8.33 kJ/cm; C — light micrograph of the weld produced at a heat input of 4.49 kJ/cm. Etchant: Ammonium hydroxide solution.

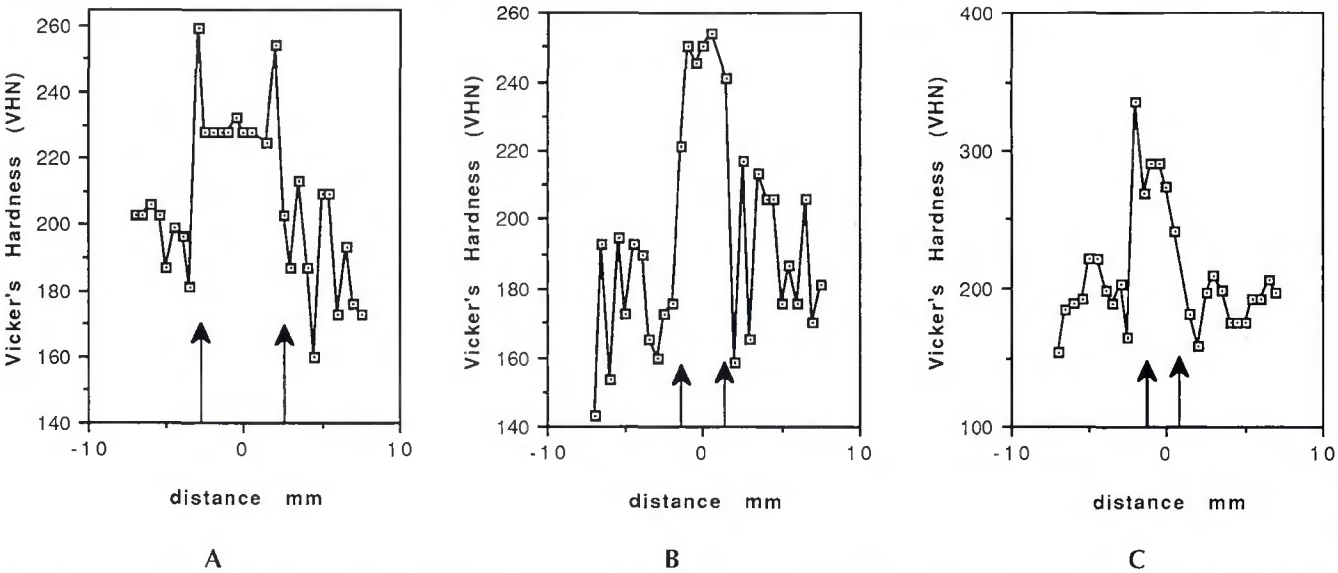

Fig. 12 — Vicker's hardness profile for the weld produced at a heat input of A — 12.52 kJ/cm, B — 8.33 kJ/cm, and C — 4.49 kJ/cm. (0 mm signifies the weld center.)

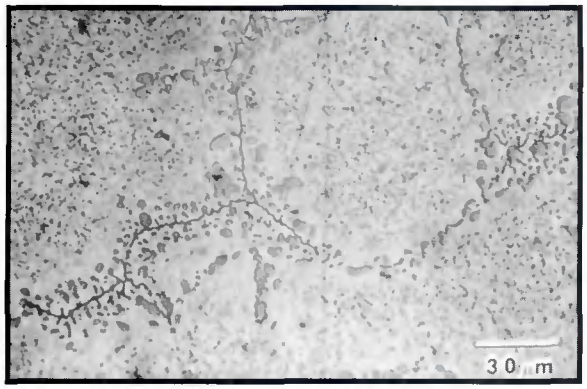

Fig. 13 — Light micrograph of the furnace cooled NAB material. Etchant: Ammonium hydroxide solution.

correspond respectively to the martensite found in the HAZ.

A Preliminary Study of Continuously Cooled NAB Material

In an effort to understand the phase transformations that occur in this material in further detail, it was decided to attempt to transform the material completely to the β phase, followed by continuous cooling which would give rise to the α phase, together with the various κ phases. It was found that a heat treatment of 120 min at 1000°C ±2° yielded 100% β. This is consistent with earlier work by, *e. g.,* Jahanafrooz, *et al.,* 1983. Quenching in ice-water produced martensite together with Widmanstätten proeutectoid α. Air cooling produced proeutectoid α together with the eutectoidal mixture of $\alpha + \kappa_{iii}$. Furnace cooling produced the same constituents but on a coarser scale. Figure 13 is a light micrograph of the furnace cooled material. As can be seen, there is no grain boundary between the proeutectoid α and the eutectoidal α, *i.e.,* they are of the same orientation. This implies that the proeutectoid α initiated the eutectoid reaction and may be termed the active nucleus for the eutectoidal mixture of $\alpha + \kappa_{iii}$.

Conclusions

In summary, laser beam welding is very effective in producing narrow heat affected zones in the NAB material. The objective of attaining full penetration of the plate was accomplished in 54% of the weldments. Further experimentation, including a more intensive study concerning the effects of the laser beam welding parameters on this material, is necessary to consistently obtain full-penetration weldments.

This study also verified that microstructural banding is present in the base plate and exists through the HAZ to the fusion line. The base plate contains alternating bands of the copper-rich solid solution, *i.e.,* proeutectoid α, and the eutectoid mixture of $\alpha + \kappa_{iii}$. κ_{iv} is also present in the base plate, both within the proeutectoid α grains and along the proeutectoid α grain boundaries. It was also evident that a large fraction of proeutectoid α and the eutectoid mixture $\alpha + \kappa_{iii}$ transforms to martensite in the HAZ. Columnar grains of the weld metal (consisting of Widmanstätten proeutectoid α and martensite) exist adjacent to the fusion line; however, the grains attained an equiaxed morphology as the centerline of the weld metal is approached. The phases present at the weld center are primarily Widmanstätten proeutectoid α and martensite. Welds produced at lower heat inputs exhibited a finer microstructure in the weld metal when compared with those which were produced at higher heat inputs.

The microhardness data revealed that the weld metal and HAZ were hard relative to the base plate. The stray peaks, as mentioned above, are a result of a measurement being recorded on the martensite found in the HAZ.

Aknowledgments

Special thanks to Terri Marsico of the Applied Research Laboratory and Dr. Paul R. Howell of the Materials Science and Engineering Department for their continuous support and assistance.

References

1. Bell, D. E., Marsico, T. A., Petrolonis, K., Denney, P. E., and Howell, P. R. The Microstructure of Laser-Welded Aluminum Bronzes. ASTM paper, Symposium: Metallography 75 years later, 1991, in press.

2. Bell, D. E., MS Thesis. Microstructural Development and Corrosion Resistance of Laser Welded Nickel-Aluminum Bronze. The Pennsylvania State University, August 1993.

3. Cook, M., Fentimen, W. P., and Davies, E. *J. Inst. Met.,* 80(1951-1952): 419.

4. Culpan, E. A., and Foley, A. G. The Detection of Selective Phase Corrosion in Cast Nickel Aluminum Bronze by Acoustic Emission Techniques. *J. Mat. Sci.* 17(1982):953-964.

5. Fontana, M. G. *Corrosion Engineering,* 3rd edition, McGraw-Hill Book Company, 1986, 86-90.

6. Hasan, F., Lorimer, G. W., and Ridley, N. Phase Transformations During Welding of Nickel-Aluminum-Bronze. In Proc. Conf. on Phase Transformations, Cambridge, U. K., July 1987, 131-34.

7. Hasan, F., Lorimer, G. W., and Ridley, N. Crystallography of Martensite in a Cu-10Al-5Ni-5% Fe Alloy. *J. de Physique,* 43, December 1982, C4-653-658.

8. Jahanafrooz, A., Hasan, F., Lorimer, G. W., and Ridley, N. Microstructural Development in Complex Nickel-Aluminum-Bronzes. *Met. Trans. A,* 14A (1983), 1951-1956.

9. Lancaster, J. F. *Metallurgy of Welding,* 4th edition, Allen and Unwin, London, 1980, 43-51.

10. Lorimer, G. W., Hasan, F., Iqbal, J., and Ridley, N. Observation of Microstructure and Corrosion Behavior of Some Aluminum Bronzes. *Br. Corrosion J.,* 1986, 21, No. 4, 244–248.

11. Petrolonis, K. MS thesis, Laser Welding and Continuous Cooling Studies of Nickel-Aluminum Bronze. The Pennsylvania State University, August 1993.

12. Thompson, S. W., and Howell, P. R. Banding and the Origin of Large Pearlite Nodules in a Low-Alloy Plate Steel Containing 0.15 WT PCT Carbon. *Mat. Sci. Tech.,* 8(1992), 777.